Synergetic Catalytic Effect of Cu$_{2-x}$Se Nanoparticles and Reduced Graphene Oxide Coembedded in Electrospun Nanofibers for the Reduction of a Typical Refractory Organic Compound

Tong Yang,[†] Hong Yan Zou,[‡] and Cheng Zhi Huang*,[†,‡]

[†]Key Laboratory of Luminescent and Real-Time Analytical Chemistry (Southwest University), Ministry of Education, School of Chemistry and Chemical Engineering, Southwest University, Chongqing 400715, P. R. China

[‡]College of Pharmaceutical Science, Southwest University, Chongqing 400716, P. R. China

Ⓢ *Supporting Information*

ABSTRACT: A new heterogeneous catalytic composite composed of nonstoichiometric Cu$_{2-x}$Se nanoparticles (NPs) with high copper deficiency and graphene oxide (GO) is prepared by coembedding in electrospun nanofibers of a poly-(vinylpyrrolidone) (PVP) support, wherein GO in the nanofibers is converted into reduced GO (rGO) via heat treatment. The as-prepared composite Cu$_{2-x}$Se/rGO/PVP nanofibers have demonstrated superior catalytic activity toward the reduction of a refractory organic compound by taking 4-nitrophenol (4-NP) as an example. In the presence of NaBH$_4$, the Cu$_{2-x}$Se/rGO/PVP nanofibers display a synergetic effect between Cu$_{2-x}$Se and rGO in PVP nanofibers compared to their independent components or corresponding nanofibers. Furthermore, the Cu$_{2-x}$Se/rGO/PVP nanofibers exhibit a favorable water-stable property via heat treatment to solidify the hydrophilic PVP matrix, which makes the composite display good reusability, stability in aqueous solution, and separability from a water medium. This work not only presents a direct, convenient, and effective approach to doping semiconductor nanomaterials into polymer nanofibers but also provides fundamental routes for further investigations about the synergetic effect between different materials based on the platform of electrospun nanofibers.

KEYWORDS: synergetic effect, Cu$_{2-x}$Se and rGO, electrospun nanofibers, catalytic reduction, 4-nitrophenol
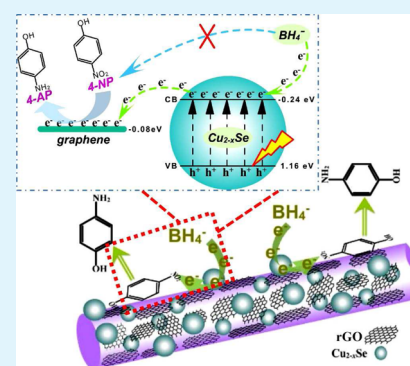
■ INTRODUCTION

Increasing environmental protection demands have stimulated wide research on the design and fabrication of many catalysts that are low cost, highly efficient, and environmentally friendly in catalytic energy conversion reactions.[1,2] A variety of nanostructure catalysts such as single noble-metal nanoparticles (NPs),[3] bimetallic nanocomposites,[4,5] core–shell microgels,[6] and semiconductor heterostructures[7] have been used in catalytic chemistry. Among these nanomaterials, bifunctional composites exhibit excellent catalytic performance because of the synergetic effect between the components. However, the small-size effect of nanocatalysts will be tediously separated from an aqueous medium to reduce their recycling rate and easily aggregate to minimize their surface area, resulting in low catalytic efficiency. Thus, it is a good choice that the nanostructures or functional molecules are well-distributed in supports—polymer nanofibers—by electrospinning.

Electrospinning has been recognized as one of the most outstanding and versatile techniques to prepare nonwoven, continuous, and functional nanofibers with diameters ranging from nanometers to a few micrometers.[8–11] For improving the functionality and wide application of electrospun nanofibers, exciting methods including doping of various functional molecules into nanofibers and modification of the as-prepared

nanofibers were adopted and further applied in numerous fields such as sensing,[9,12–14] separation through filtering and adsorption,[15,16] energy and environment,[17,18] smart materials and imaging,[19,20] and biomedicine.[21,22] One of the most remarkable and straightforward advantages of electrospinning is that the electrospun nanofibers can be applied in catalytic fields because (1) the electrospun polymer nanofibers could prevent functional molecules or NPs immobilized on them from aggregating and the catalytic components could be further preserved,[13,23] (2) the large surface area to volume ratio and high porosity could provide catalytic reactions with an adequate space,[24,25] and (3) the nanofibrous morphology and excellent mechanical properties are superior to those of individual NPs because of their recyclability, reusability, and environmental friendliness.[26] Therefore, developing a new composite of electrospun nanofibers as catalysts for the reduction of refractory organic compounds such as 4-nitrophenol (4-NP) may generate more upsurges in the area of environmental treatment.

At present, berzelianite Cu$_{2-x}$Se, a self-doped semiconductor copper chalcogenide nanomaterial, has been found to present

excellent catalytic activity.[27] Owing to the high concentration of free carriers in $Cu_{2-x}Se$ NPs ascribed to high copper deficiency, $Cu_{2-x}Se$ NPs have both good electron donors and acceptors with high ionic mobility and thus show greatly enhanced catalytic ability by facilitating electron transfer.[27] Further investigations showed that $Cu_{2-x}Se$/reduced graphene oxide (rGO) composites, which were prepared by combining $Cu_{2-x}Se$ with a carbon nanomaterial and supplied a good pathway for increasing the density of free carriers in the valence band in $Cu_{2-x}Se$ NPs, have strong and tunable near-infrared (NIR) absorption, extending the photocatalytic wavelength range of sunlight.[28]

Graphene, as a rapidly rising star material, exhibits excellent synergetic catalytic abilities in accordance with other composites owing to its unique properties such as superior charge mobility, high specific surface area, nanostructure of sp^2sp^3 hybrid carbon network with plentiful oxygen-containing groups, and $\pi-\pi$-conjugated structure.[29−32] However, many semiconductor/ graphene, rGO, or graphene-like nanocomposite materials have focused on the degradation of dyes, pollutants, and volatile organic pollutants, the destruction of microorganisms, and water splitting by a synergetic photocatalytic effect.[31,33,34] On the other hand, researches on making the best of the synergetic effect between a semiconductor nanomaterial and graphene catalysts for direct catalytic redox reaction are relatively limited. In addition, because of the high cost, tedious preparation process, and limited supply, improvement of the catalytic efficiency is vital for practical applications. Hence, on the basis of the electrospun nanofibers as a platform, it is a perfect choice that the metallic NPs/graphic or carbon nanofibers were applied in the catalytic area. In a similar way, the combination of $Cu_{2-x}Se$ NPs and rGO might provide a basic guarantee for catalytic reaction.

With this purpose, we herein for the first time fabricated the $Cu_{2-x}Se$/rGO nanofibers by a PVP solution blend of $Cu_{2-x}Se$ NPs and GO. Then, the composite electrospun nanofibers underwent heat treatment to solidify the PVP polymer matrix and prepare a doping graphene and water-stable nanofibers. What is more, it was found that the as-fabricated $Cu_{2-x}Se$/rGO/ PVP composite nanofibers exhibited enhanced catalytic activity toward the reduction of 4-NP to 4-aminophenol (4-AP) in the presence of $NaBH_4$ compared with independent $Cu_{2-x}Se$ NPs or rGO nanofibers because of the synergetic effect between them. These water-stable nanofibers displayed a favorable reusability, stability in aqueous solution, and separability from water solution. Finally, it was also uncovered that electrospun nanofibers could provide a good support for improving the catalytic efficiency compared to individual $Cu_{2-x}Se$ NPs and a GO solution.

EXPERIMENTAL SECTION

Materials. Copper sulfate ($CuSO_4·5H_2O$; Regent Chemical Reagent Co., Ltd., Tianjin, China) was of analytical grade. Ascorbic acid (AA) was obtained from Dingguo Changsheng Biotechnology Co., Ltd. (Beijing, China). Poly(vinylpyrrolidone) powder (PVP; average M_w = 1 300 000), 4-nitrophenol (4-NP, 99.9%), and selenious dioxide (SeO_2, 99.9%) were supplied by Aladdin Chemistry Co., Ltd. (Shanghai, China). PVP (average M_w = 55000) was purchased from Sigma-Aldrich. GO was supplied by XF NANO Inc. (Nanjing, China) and dissolved on deionized water (DIW) via sonication for a desired time. Absolute ethanol (C_2H_5OH, 99.7%) and sodium borohydride ($NaBH_4$) were acquired from Amresco Co. All chemicals were used as received unless specified otherwise.

Synthesis of $Cu_{2-x}Se$ NPs. The $Cu_{2-x}Se$ NPs stabilized with PVP (M_w = 55000) were synthesis according to our previously reported method.[27] Minutely, 30.0 mg of PVP was totally dissolved in 10 mL of

DIW in a round-bottomed flask. Then SeO_2 (0.25 M, 0.5 mL) and AA (0.2 g/mL, 0.2 mL) were added to the PVP solution in order. After 10 min, the yellow-green preblended solution of $CuSO_4·5H_2O$ (0.5 M, 0.5 mL) and AA (0.2 g/mL, 0.3 mL) was added, in which AA reduced Cu^{2+} to Cu^+. The entire reaction was allowed to proceed under vigorous stirring in a 40 °C water bath for 6 h to finally gain an atrovirens suspension solution, indicating that $Cu_{2-x}Se$ NPs stabilized with PVP was produced. The products were centrifuged for 10 min at 10000 rpm, washed, and resuspended in DIW three times. Finally, the products remained an anatrovirens solution and were stored at 4 °C in a refrigerator before use.

Preparation of Different Electrospun Solutions. PVP (9 wt %, M_w = 1 300 000), as a polymer matrix, was prepared by dissolving in an appropriate amount of C_2H_5OH under vigorous stirring. First, the GO aqueous solution was added into a PVP viscous solution under magnetic stirring to obtain a light-brown, transparent, and homogeneous GO/ PVP polymer solution, in which the mass ratios of GO and PVP were 2:500, 1.5:500, 1:500, and 0.5:500 (mg:mg). Second, the $Cu_{2-x}Se$ NP aqueous solution were centrifuged for 10 min at 10000 rpm, and the precipitation was moved into a PVP viscous solution under magnetic stirring to gain an atrovirens $Cu_{2-x}Se$/PVP polymer solution. Third, the GO aqueous solution and $Cu_{2-x}Se$ NPs were successively added to a PVP polymer solution. The atrovirens $Cu_{2-x}Se$/GO/PVP electrospun solutions were acquired under vigorous stirring for several hours.

Electrospinning and Pretreatment of Composite Nanofibers. The above viscous solutions were filled into three 10 mL plastic syringes with 0.8-mm-diameter blunt-ended needles. The GO/PVP, $Cu_{2-x}Se$/ PVP, and $Cu_{2-x}Se$/GO/PVP electrospun nanofibers were fabricated by using commercial electrospinning equipment (DNF-001, Beijing Kaiweixin Technology Co. Ltd., China). All nanofibers were electrospun under a high voltage of 20.0 kV, and the needle was located at a distance of 20 cm from the ground collector and wrapped in aluminum foil. The syringe pump was applied to feed solutions to the needle at a rate of 1.8 mm/h. Last, in order to obtain water-stable nanofibrous membranes, all fresh composite electrospun membranes were allowed to solidify at 200 °C for 1 h in a muffle furnace and removed the remanent solvent for characterization and subsequent catalytic experiments. At the same time, the rGO and $Cu_{2-x}Se$/rGO nanofibers were prepared.

Chatacterization. The morphologies and diameters of the $Cu_{2-x}Se$ NPs and as-prepared composite nanofibers were observed by scanning electron microscopy (SEM; S-4800, Hitachi Ltd., Tokyo, Japan) and transmission electron microscopy (TEM), with the transmission electron microscope attached to the scanning electron microscope. The elemental composition of the samples was analyzed using an energy-dispersive X-ray (EDX) spectroscopic detector attached to the scanning electron microscope. The UV−vis absorption spectra of $Cu_{2-x}Se$ NPs were measured with an UV-3600 spectrophotometer (Hitachi Ltd., Tokyo, Japan). Powder X-ray diffraction (XRD) patterns were obtained by a Shimadzu XRD-7000 diffractometer (Beijing Purkinje General Instrument Co., Ltd.) with a Cu $K\alpha$ (1.5405 Å) radiation source under an operating voltage and current of 40 kV and 50 mA, respectively. X-ray photoelectron spectroscopy (XPS) analysis was performed on an ESCRLRB 250 X-ray spectrometer (America) with a standard Al K source ($h\nu$ = 1486.6 eV). Functional-group analysis of fibrous mats was recorded by a Fourier transform infrared (FTIR) spectrometer (8400S; Shimadzu, Kyoto, Japan) from 4000 to 600 cm^{-1} at room temperature. Measurement of the GO spectra was performed on a LabRAM-HR Raman spectrometer (HORIBA Jobin Yvon, Villeneuve-d'Ascq, France) with an excitation source that was 532 nm using an accumulation time of 5 s. The specific surface area, porosity, and pore size distribution of the samples were analyzed by the Brunauer− Emmett−Teller (BET) method, using a surface area analyzer (Quantachrome Autosorb-1, USA) with 100 mg of each sample, which had been dried for 6 h at 60 °C.

Catalytic Reduction of 4-NP. In order to study the synergetic catalytic activity of $Cu_{2-x}Se$ NPs and rGO in electrospun nanofibers, the reduction of 4-NP to 4-AP in the presence of $NaBH_4$ was employed as a model reaction.

The typical reduction reaction does not occur without catalysts because of the kinetic barrier caused by the large potential difference

between the donor and acceptor molecules.[35] Thus, 50.0 mg of composite nanofibrous catalysts was added to the mixed solution containing 19.5 mL of DIW, 4-NP (10 mM, 250 μL), and NaBH$_4$ (5 M, 250 μL) with continuous stirring in a round-bottomed flask in a 25 °C water bath, wherein the amount of NaBH$_4$ during this whole reaction was in high excess to ensure the assumption of pseudo-first-order kinetics with respect to the catalytic reduction of 4-NP.[36] At a specific time interval, the changes of the mixed sample solutions were monitored with a UV−vis spectrophotometer upon collection in a quartz cuvette. The amounts of composite nanofibrous catalysts (Cu$_{2-x}$Se/PVP, rGO/PVP, and Cu$_{2-x}$Se/rGO/PVP) were equal in each catalytic reaction. All reactions using different catalysts were also conducted at 30, 35, and 40 °C, and the activation energies were calculated, respectively. Ultimately, in order to testify to the reusability of the Cu$_{2-x}$Se/rGO/PVP nanofibrous mats, the composite mats were collected in a funnel with filter paper, washed with DIW, and reused in the next reaction. Additionally, the water-stable property of the as-fabricated nanofibrous mats was investigated by immersion in DIW at different intervals in 7 h and characterization by SEM.

RESULTS AND DISCUSSION

Preparation of Monodispersed Cu$_{2-x}$Se NPs. The synthesis of Cu$_{2-x}$Se NPs and the formation mechanism of Cu$_{2-x}$Se NPs were amply studied in our previous research.[28] To assemble Cu$_{2-x}$Se NPs on PVP (M_w = 1 300 000) and a GO/PVP nanofibrous matrix, this work mainly adopted the synthesis step of Cu$_{2-x}$Se NPs coated with PVP (Cu$_{2-x}$Se@PVP) to fabricate Cu$_{2-x}$Se/PVP and Cu$_{2-x}$Se/GO/PVP composite nanofibers, respectively.

The morphology and composition of the as-synthesized Cu$_{2-x}$Se NPs were characterized by SEM, TEM, and EDX. It is thus clear that the Cu$_{2-x}$Se@PVP NPs were spherical, highly dispersed, and uniform (Figure 1A,B). Their average diameter
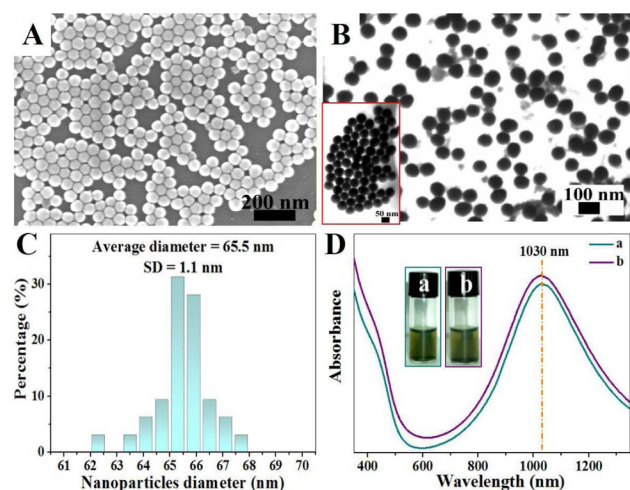

Figure 1. Characterization of the as-synthesized Cu$_{2-x}$Se NPs: (A) SEM image; (B) TEM image; (C) size distribution histogram of Cu$_{2-x}$Se NPs corresponding to the TEM image; (D) absorption spectra of Cu$_{2-x}$Se NPs with high copper vacancy from UV to NIR. Inset: new suspension solution image of Cu$_{2-x}$Se NPs (a) and that one stored at 4 °C for 2 months (b).

size is 65.5 nm by NP statistics (Figure 1C), which corresponds to the TEM image of Figure 1B. EDX analysis verified the presence of Cu, Se, C, and O elements, and the atomic ratio of Cu and Se is approximately 1.6 (x = 0.4), suggesting a high copper deficiency in Cu$_{2-x}$Se NPs (Figure S1A in the Supporting Information, SI).[27,28] Otherwise, the nonstoichiometric Cu$_{2-x}$Se NPs with high copper vacancy, which could be highly dispersed

in water, exhibited an atrovirens suspension solution and had intense absorption from the UV to NIR region (Figure 1D). NIR absorption of a Cu$_{2-x}$Se NP suspension aqueous solution centered at 1030 nm [Figure 1D(a)] shows carrier concentration-dependent plasmonic absorption.[37] The stability of Cu$_{2-x}$Se NPs stored at 4 °C was monitored by UV−vis absorption; the NIR region also presented a strong absorption peak at the same wavelength after 2 months [Figure 1D(b)], demonstrating that the template-directed synthesis route of Cu$_{2-x}$Se NPs was a well-viable project and the stability of Cu$_{2-x}$Se NPs was very good.

Fabrication of Electrospun Nanofibrous Mats. In order to enhance the good humidity resistance of PVP nanofibers as polymeric hosts in the atmosphere, the polymeric hosts were solidified by annealing.[38] Herein, the following PVP, rGO/PVP, Cu$_{2-x}$Se/PVP, and Cu$_{2-x}$Se/rGO/PVP hybrid composite nanofibers were prepared by annealing at 200 °C for 1 h.

The good morphologies of the as-prepared composite nanofibers are the strategic embodiment of electrospinning technology and could lay a good foundation for the latter catalytic experiments. First of all, the representative SEM and TEM images of the as-fabricated electrospun nanofibrous mats based on a PVP polymeric matrix exhibited uniform diameters and highly reticulate structures, which are propitious to improving the surface areas of nanofibrous mats (Figure 2A−E). The diameter size distribution histograms of only PVP, rGO/PVP, Cu$_{2-x}$Se/PVP, and Cu$_{2-x}$Se/rGO/PVP nanofibers after annealing were calculated from the relevant SEM images, whose average diameters were 325 ± 30, 356 ± 60, 354 ± 41, and 343 ± 47 nm, respectively (Figure S2 in the SI). It was clear that the diameters of the subsequent hybrid nanofibers were thicker than those of only PVP nanofibers, suggesting that the viscosity of the electrospun solution would be changed with the addition of GO and a Cu$_{2-x}$Se NP suspension solution in a PVP polymeric solution.[9,21] Compared with these nanofibers after annealing, the diameters of the corresponding nanofibers before annealing were thicker as well (Figure S3A−D in the SI). Besides, it is obvious that these nanofibrous mats after annealing were independent rather than adherent between nanofibers. This can be ascribed to the shrinking of the nanofibers with evaporation of remanent solvent at higher temperature, which could solidify the hybrid nanofibers to form a water-stable material. Figure 2E shows that the diameter of Cu$_{2-x}$Se NPs on nanofibers after annealing was about 65.0 nm, in agreement with the preceding statistics in Figure 1C. At the same time, it was proved that the morphology of Cu$_{2-x}$Se NPs on rGO/PVP was still a sphere after annealing in the TEM image (Figure 2F). The above results demonstrate that the morphologies of these hybrid composite nanofibers could be controlled and the spheres of Cu$_{2-x}$Se NPs could be destroyed at higher temperature.

Comparative optical photographs of only PVP, GO/PVP, Cu$_{2-x}$Se/PVP, and Cu$_{2-x}$Se/GO/PVP nanofibrous membranes before and after heat treatment are presented in Figure S4A−D in the SI. This reveals that the colors of these nanofibrous membranes are darker after annealing. The results imply that annealing certainly has as a key role in solidifying the PVP polymer matrix and in forming water-stable electrospun nanofibrous materials.

Structural Characterization of Cu$_{2-x}$Se NP-Loaded Electrospun Membranes. To further explore the crystal and components of the Cu$_{2-x}$Se NP-loaded electrospun nanofibers, XRD, XPS, and EDX of the as-prepared eletrospun nanofibers were performed.
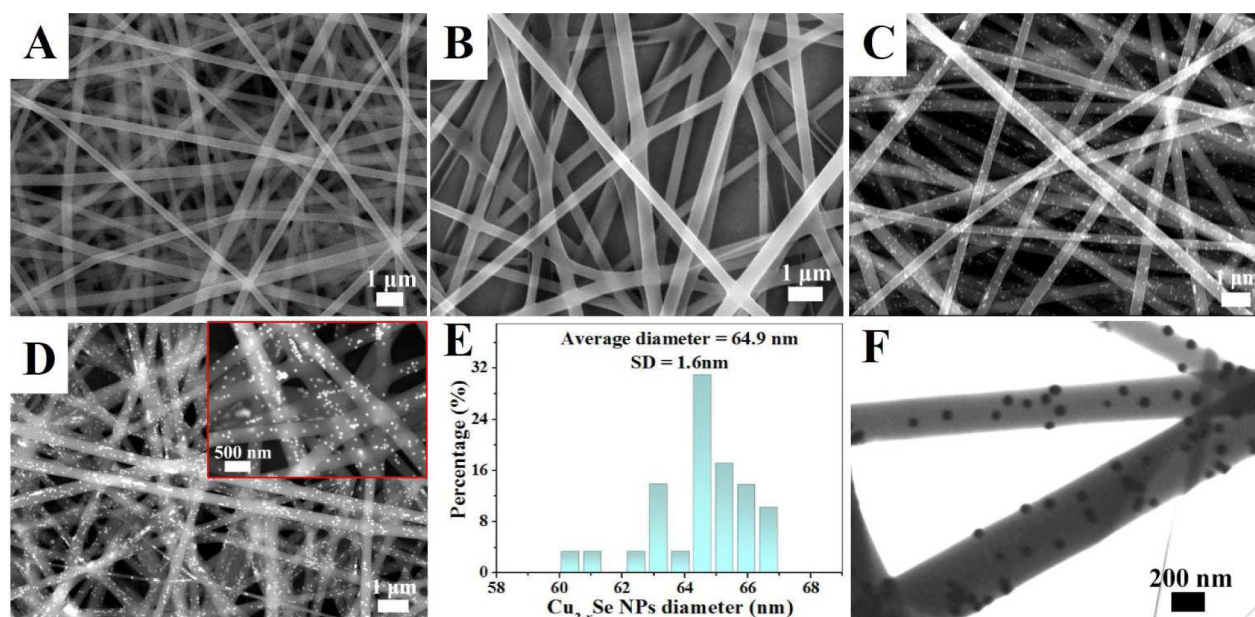
Figure 2. Morphologies of the as-prepared corresponding electrospun nanofibers characterized by SEM and TEM. The SEM images of the nanofibers are for (A) only PVP, (B) rGO/PVP, (C) $Cu_{2-x}Se/PVP$, and (D) $Cu_{2-x}Se/rGO/PVP$. (E) Size distribution histograms of $Cu_{2-x}Se$ NPs on rGO/PVP nanofibers corresponding to the magnified SEM image of the top right insert of image D. (F) TEM image of $Cu_{2-x}Se/rGO/PVP$ nanofibers after calcination.
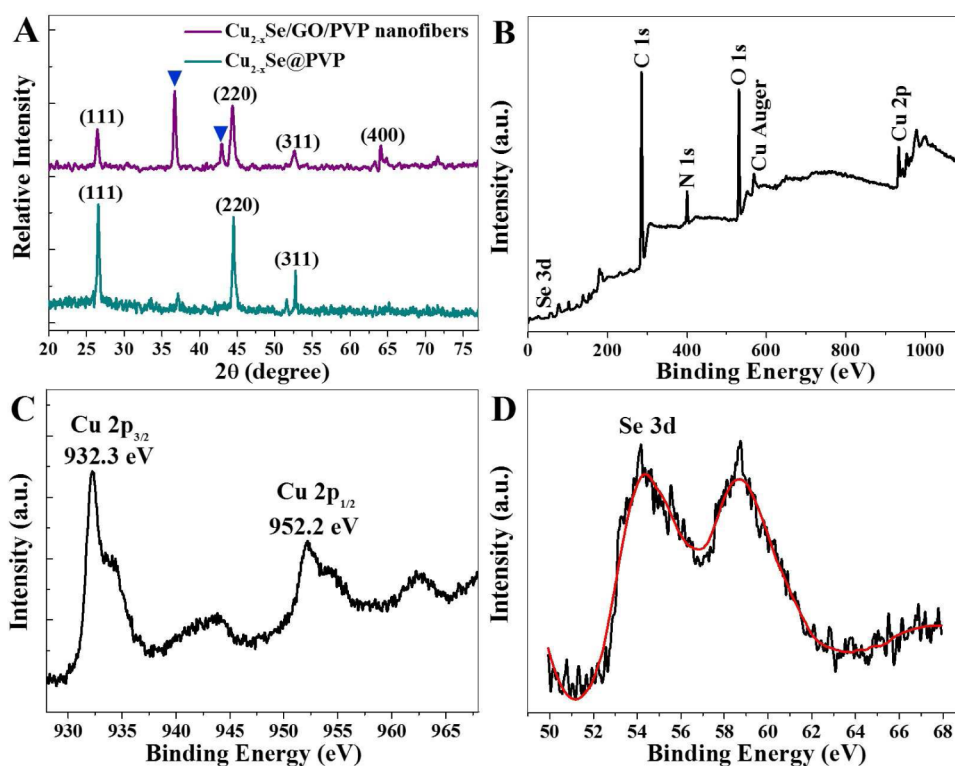

Figure 3. Characterization of the as-prepared fresh $Cu_{2-x}Se@PVP$ NPs and $Cu_{2-x}Se$ NPs on the rGO/PVP nanofibers. (A) XRD patterns of fresh $Cu_{2-x}Se@PVP$ NPs (dark cyan curves) and $Cu_{2-x}Se$ NPs on the rGO/PVP nanofibers (purple curves). (B) XPS fully scanned spectra of $Cu_{2-x}Se/rGO/PVP$ nanofibers. XPS spectra of (C) Cu 2p and (D) Se 3d.

Figure 3A shows the XRD patterns of the only $Cu_{2-x}Se@PVP$ NPs and $Cu_{2-x}Se/rGO/PVP$ composite nanofibrous mats. The characteristic diffraction peaks with 2θ values on $Cu_{2-x}Se@PVP$ NPs centered at around 26.8°, 44.6°, and 53.0° respectively correspond to the (111), (220), and (311) planes of the cubic phase $Cu_{2-x}Se$ (Figure 3A, dark-cyan curve).[27,28,39] The typical

XRD pattern of the $Cu_{2-x}Se/rGO/PVP$ composite nanofibrous mats after annealing shows that the diffraction peaks with 2θ values located at 26.5°, 45.0°, 52.6°, and 64.8° are consistent with the (111), (220), (311), and (400) planes of $Cu_{2-x}Se$, respectively,[27,28,40] whereas the diffraction peaks obtained near or at 36.8° and 42.8° can be assigned to the (111) and (200)

planes of Cu_2O (blue triangle block in Figure 3A).[41,42] We suppose that the Cu_2O species forms a thin layer at the surface of $Cu_{2-x}Se$ NPs, resulting from the interaction between Cu^+ in $Cu_{2-x}Se$ NPs and O in nanofibers. The chemical composition and valent state of the $Cu_{2-x}Se$/rGO/PVP composite nanofibrous mats were analyzed by XPS and EDX. As can be seen from Figure 3B, the fully scanned spectra of $Cu_{2-x}Se$/rGO/PVP composite nanofibrous mats after annealing obviously presents the binding energies of C 1s, N 1s, O 1s, Cu 2p, and Se 3d. C 1s, N 1s, and O 1s chiefly were from PVP and rGO. The high-resolution XPS spectra of the Cu 2p orbital region show the binding energies of the Cu $2p_{3/2}$ and Cu $2p_{1/2}$ peaks at 932.3 and 952.2 eV, corresponding to either Cu^0 or Cu^+, while the peaks of Cu 2p at 940.0−945.0 eV were attached to Cu^{2+} (Figure 3C).[27,40] The main XPS peak of Se 3d at 54.4 eV is due to Se^{2-}, and the peak at 58.7 eV is on behalf of the oxidation state of Se (Figure 3D).[28] It is verified that Cu^+ and Se^{2-} in $Cu_{2-x}Se$ might be partially oxidized upon annealing. At the moment, the elemental compositions of $Cu_{2-x}Se$ NPs and $Cu_{2-x}Se$/rGO/PVP composite nanofibrous mats before and after were also determined by EDX, which also confirmed the presence of Cu, Se, C, and O elements (Figure S1 in the SI). The results showed that the atom ratios of $Cu_{2-x}Se$ NPs and $Cu_{2-x}Se$/rGO/PVP nanofibers before and after annealing were about 1.70 ($x = 0.30$), 1.66 ($x = 0.34$), and 1.60 ($x = 0.40$), respectively, implying that $Cu_{2-x}Se$ NPs still maintain the structure of high copper vacancy after electrospinning and post-treatment.[27,43] The above all mainly demonstrate the successful assembly of $Cu_{2-x}Se$ on the rGO/PVP hybrid nanofibrous mats.

In addition, GO as a crucial doped component in nanofibers might be reduced to rGO, which was characterized by FTIR analysis and Raman spectrometry. Figure 4A shows the FTIR spectra of PVP powder, pure GO, rGO/PVP, $Cu_{2-x}Se$/rGO/PVP, and $Cu_{2-x}Se$/PVP nanofibers after calcination, respectively. The peaks for pure PVP at 1653 and 1290 cm^{-1} were assigned to the carbonyl group (C═O asymmetric stretching) and acid amides in pyrrolidone. The peaks of oxygen-containing functional groups in pure GO include the stretching vibration of the hydroxyl group (−OH) at 3426 cm^{-1}, the asymmetric and symmetric stretching vibrations of conjugated carbonyl groups (−C═O) or carboxyl groups (−COOH) on the edges of the basal planes at 1725, 1632, and 1358 cm^{-1}, and the stretching vibration of C−O at 1090 cm^{-1} successively. There are not many characteristic peaks about GO in $Cu_{2-x}Se$/PVP nanofibers. However, the two oxygen-containing characteristic absorption peaks at 1725 cm^{-1} (−C═O) and 1090 cm^{-1} (C−O) disappear for rGO/PVP and $Cu_{2-x}Se$/rGO/PVP nanofibers after annealing, which showed that GO might be reduced in nanofibers. To further demonstrate whether GO was doped into relevant nanofibers and the heat treatment could efficiently reduce GO to rGO, the Raman spectra of only GO, rGO/PVP, $Cu_{2-x}Se$/rGO/PVP, and $Cu_{2-x}Se$/PVP nanofibrous mats were confirmed from Figure 4D. As shown Figure 4D(a), the D band at approximately 1353 cm^{-1} arises from the edge effect and the disordered aromatic structure of GO and the G band at approximately 1598 cm^{-1} appears because of the vibration of the sp^2-bonded C atoms.[44] Similarly, both rGO/PVP and $Cu_{2-x}Se$/rGO/PVP composite nanofibrous mats also exhibit two characteristic main bands, but the two bands were absent in $Cu_{2-x}Se$/PVP nanofibrous mats. Notably, the intensity ratio of the D and G bands (I_D/I_G) is a measure of the relative concentration of local defects or disorders compared with sp^2-hybridized graphene domains.[44] It is apparent from Figure 4D that I_D/I_G is 1.04 for
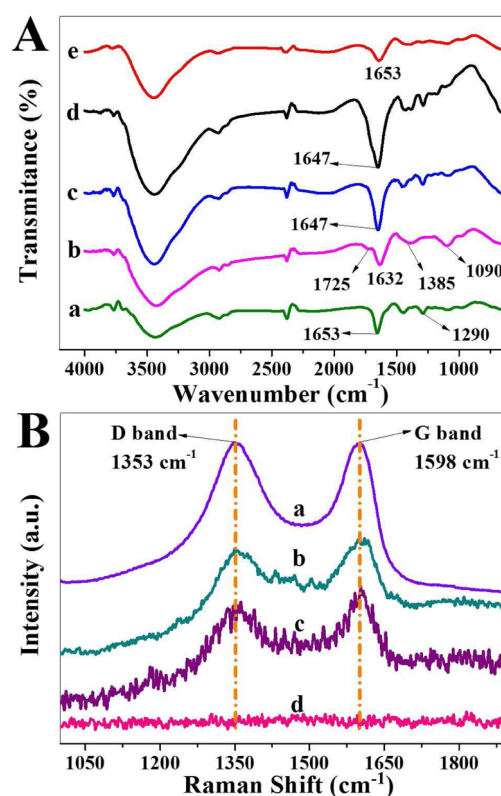

Figure 4. Characterization of GO in hybrid nanofibers. (A) FTIR spectra of pure PVP (a), pure GO (b), rGO/PVP nanofibers (c), $Cu_{2-x}Se$/rGO/PVP nanofibers (d), and $Cu_{2-x}Se$/PVP nanofibers (e). (B) Raman spectra of GO (a), rGO/PVP nanofibers (b), $Cu_{2-x}Se$/rGO/PVP (c), and $Cu_{2-x}Se$/PVP nanofibers (d). Laser wavelength: 532 nm. Power: 28 mW. Lens: 50× objective. Acquisition time: 5 s.

GO. After calcination, the I_D/I_G ratios of rGO/PVP and $Cu_{2-x}Se$/rGO/PVP nanofibers are decreased to 0.95 and 0.92, respectively, which is attributed to more graphitization of the nanocomposite fibers with the calcination process. From the above results, it is demonstrated that (a) GO was successfully doped in rGO/PVP and $Cu_{2-x}Se$/rGO/PVP nanofibers and (b) GO in nanofibers under the condition of 200 °C was reduced to rGO.

Catalytic Properties of Composite Nanofibrous Mats for the Reduction of 4-NP. 4-NP is the most ordinary organic pollutant and carcinogenic to humankind and wildlife, while its amino derivative, 4-AP, is a potential intermediate for analgesic and antipyretic drugs, a corrosion inhibitor, a photographic developer, an antioxidant, and so on.[45] Otherwise, the typical reaction on the reduction of 4-NP to 4-AP in the presence of $NaBH_4$ is a thermodynamically feasible process in accordance with their standard electrode potential (E^θ) versus normal hydrogen electrode for 4-NP/4-AP = −0.76 V and H_3BO_3/BH_4^- = −1.33 V, but it is kinetically restricted without catalysts because of a kinetic barrier arose from the large potential.[46] Thus, it is of great significance to catalyze this typical reaction through the design of appropriate catalysts.

In this work, the catalytic activity of $Cu_{2-x}Se$/rGO/PVP nanofibrous mats was investigated by the reduction of toxic 4-NP to 4-AP in the presence of $NaBH_4$ as a typical model reaction, which was monitored by UV−vis spectroscopy. Normally, the characteristic absorption of a 4-NP solution is at 317 nm (Figure 5A, curve a). However, the maximum peak at 317 nm immediately red-shifted to 400 nm after the addition of a
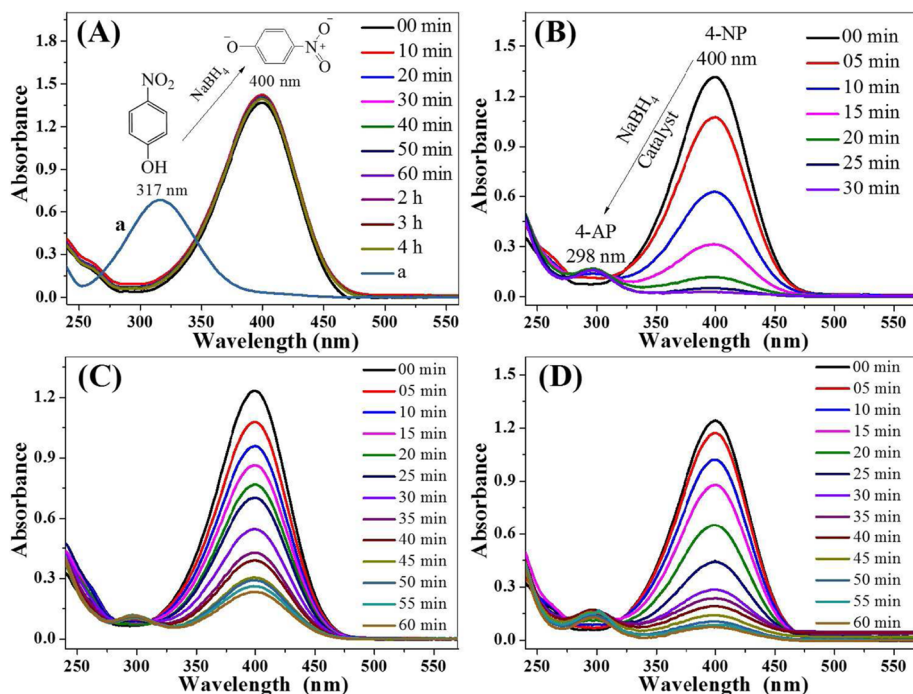
Figure 5. Catalytic performance of as-prepared nanofibrous catalysts. The reduction of 4-NP in the presence of NaBH$_4$ was monitored by UV−vis spectroscopy: (A) without any catalysts and the only 4-NP solution without NaBH$_4$ (curve a); (B) Cu$_{2−x}$Se/rGO/PVP (the mass ratio of GO and PVP was 1:500) nanofibrous catalyst; (C) Cu$_{2−x}$Se/PVP nanofibrous catalyst; (D) GO/PVP (1:500) nanofibrous catalyst.

NaBH$_4$ solution, and the color of the aqueous solution altered from pale yellow to deep yellow, which was attributed to the formation of 4-nitrophenolate ions under alkaline conditions. Upon the addition of a Cu$_{2−x}$Se/rGO/PVP nanofibrous composite catalyst, the intensity of the absorption peak at 400 nm decreased with the reaction time, and a new absorbance peak for the formation of 4-AP at 298 nm developed gradually (Figure 5B).[47] At the same time, the deep-yellow 4-nitrophenolate solution completely faded in 30 min, indicating the completion of this process (Figure S6C in the SI). For the sake of exploring the synergetic effect catalytic ability of Cu$_{2−x}$Se NPs and rGO in electrospun nanofibers, we studied the catalytic property of mono-Cu$_{2−x}$Se/PVP nanofibers (Figure 5C), rGO/PVP nanofibers (Figure 5D), Cu$_{2−x}$Se NPs (Figure S5A in the SI), and GO (Figure S5B, in the SI), respectively. From these time-dependent UV−vis absorption spectra, it is obvious that the catalytic time of Cu$_{2−x}$Se/rGO/PVP nanofibers is shorter than those of the Cu$_{2−x}$Se/PVP and rGO/PVP nanofibers, which suggested that the catalytic ability of Cu$_{2−x}$Se/rGO/PVP nanofibers is highly enhanced compared with those of the Cu$_{2−x}$Se/PVP and rGO/PVP nanofibers.

Additionally, the catalytic reduction of 4-NP by the Cu$_{2−x}$Se/PVP nanofibers and Cu$_{2−x}$Se/rGO/PVP with different weight additions of GO (2.0, 1.5, 1.0, and 0.5 mg) was investigated (Figure 6A). Significantly, the introduction of a suitable amount of GO in a Cu$_{2−x}$Se/PVP matrix can result in an obvious catalytic efficiency for 4-NP. At the same time points, the catalytic reductive efficiency of 4-NP follows the order Cu$_{2−x}$Se/rGO/PVP (the mass ratio of GO to PVP was 2:500, mg:mg) > Cu$_{2−x}$Se/rGO/PVP (1:500) > Cu$_{2−x}$Se/rGO/PVP (1.5:500) > Cu$_{2−x}$Se/rGO/PVP (0.5:500) > Cu$_{2−x}$Se/PVP, which could further testify the synergetic effect between Cu$_{2−x}$Se and rGO in the PVP matrix. In this catalytic reaction, the concentration of NaBH$_4$ is much higher than that of 4-NP [c(NaBH$_4$)/c(4-NP) = 500], which can be considered as a pseudo-first-order
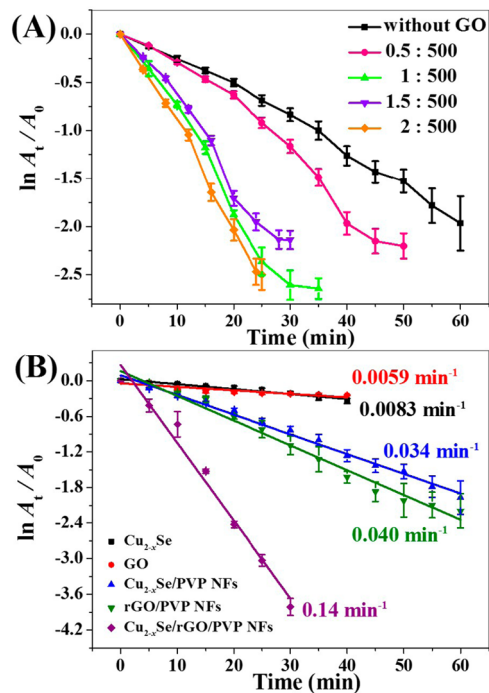

Figure 6. Plot of ln(A_t/A_0) versus time for the reduction of 4-NP with different catalysts. (A) Catalytic reduction of 4-NP over mono-Cu$_{2−x}$Se/PVP nanofibers and Cu$_{2−x}$Se/rGO/PVP nanofibers with different weight additions of GO (the mass ratios of GO and PVP were 2:500, 1.5:500, 1:500, and 0.5:500, respectively). (B) Rate constants of the catalytic reductive reaction of 4-NP obtained with different catalysts through a plot of ln(A_t/A_0) versus time from top to bottom: Cu$_{2−x}$Se NPs (black line), GO (red line), Cu$_{2−x}$Se/PVP nanofibrous mats (blue line), rGO/PVP nanofibrous mats (green line), and Cu$_{2−x}$Se/rGO/PVP nanofibrous mats (purple line) successively. Error bars represent the standard deviation of three measurements.
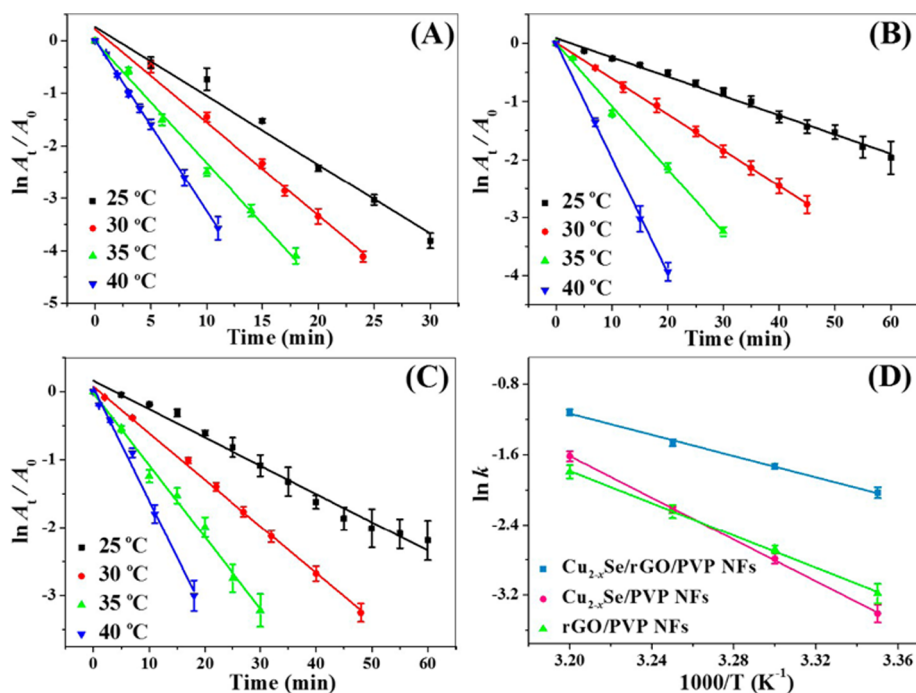
Figure 7. Kinetic study of the catalytic reductive reaction of 4-NP obtained with different catalysts and at the different temperatures. Plot of $\ln(A_t/A_0)$ versus time for the reduction of 4-NP at 25, 30, 35, and 40 °C with a $Cu_{2-x}Se/rGO/PVP$ nanofibrous catalyst (A), a $Cu_{2-x}Se/PVP$ nanofibrous catalyst (B), and a rGO/PVP nanofibrous catalyst (C). Arrhenius plots of $\ln(k)$ versus $1000/T$ for the reduction reaction of 4-NP with $NaBH_4$ carried out at 25, 30, 35, and 40 °C and catalyzed by $Cu_{2-x}Se/rGO/PVP$, $Cu_{2-x}Se/PVP$, and rGO/PVP nanofibers (D). Error bars represent the standard deviation of three measurements.

reaction.[35,45] In this case, the rate constant for the reduction of 4-NP was evaluated by the following kinetic equation:

$$\ln(c_t/c_0) = \ln(A_t/A_0) = -kt$$

where c_0 and A_0 stand for the initial concentration and absorbance of 4-NP, respectively. c_t and A_t stand for the concentration and absorbance of 4-NP at the corresponding time, respectively, and k is the first-order rate constant, wherein c_t/c_0 was acquired from the intensity of absorption at 400 nm because the absorbance of 4-NP is proportional to its concentration in the medium. Figure 6B represents plots of $\ln(A_t/A_0)$ versus relevant reaction time for the catalytic reduction of 4-NP using $Cu_{2-x}Se$ NPs, GO, $Cu_{2-x}Se/PVP$ nanofibers, rGO/PVP (1:500) nanofibers, and $Cu_{2-x}Se/rGO/PVP$ (1:500) nanofibers as catalysts separately. As can been seen, the linear relationship between $\ln(A_t/A_0)$ and the corresponding reaction time certifies pseudo-first-order kinetics. Thus, the rate constant k can be directly achieved from the slope of the linear plots. From the slope of these rate curves, the rate constant of the catalytic reaction on $Cu_{2-x}Se/rGO/PVP$ nanofibers as the catalyst is 0.14 min^{-1}, which is higher than that of other catalysts in this experimental system. These results also confirm that the synergetic effect of $Cu_{2-x}Se$ NPs and rGO in PVP nanofibers could exhibit excellent catalytic activities.

Furthermore, the activation energy (E_a) of a catalytic reaction is an empirical parameter that exhibits the dependency between the reaction temperature and rate constant k. The relevant linear relationships between $\ln(A_t/A_0)$ and the corresponding reaction time with three different catalysts including $Cu_{2-x}Se/PVP$, rGO/PVP, and $Cu_{2-x}Se/rGO/PVP$ nanofibers are shown in Figure 7A−C (time-dependent UV−vis spectral changes in Figures S7−S9 in the SI). These catalytic reactions were studied at different temperatures: 25, 30, 35, and 40 °C. It is clear that the value of

rate constant k increases with an increase of the temperature. Additionally, E_a was calculated by the classical Arrhenius theory, and the Arrhenius equation is as follows:

$$k = Ae^{-E_a/RT}$$

$$\ln k = \ln A - \frac{E_a}{RT}$$

where k is the first-order rate constant, A is the preexponential factor, E_a is the activation energy, R is the universal gas constant, and T is the reaction temperature. The corresponding E_a values were evaluated from the slope based on the linear fitting of $\ln k$ versus $1000/T$ (Figure 7D). E_a of the $Cu_{2-x}Se/rGO/PVP$ nanofibers (49.05 ± 1.70 kJ/mol) was much lower than that of the $Cu_{2-x}Se/PVP$ (86.47 ± 1.22 kJ/mol) and rGO/PVP (77.32 ± 1.60 kJ/mol) nanofibers, demonstrating an excellent catalytic activity for the composite $Cu_{2-x}Se/rGO/PVP$ nanofibers (Table 1). All of these results indicated that $Cu_{2-x}Se$ NPs with copper deficiency and rGO in PVP nanofibers could use the synergetic effect to enhance the catalytic activity for the reduction of 4-NP.

Reaction Mechanism of the Catalytic Properties of Composite $Cu_{2-x}Se/rGO/PVP$ Nanofibrous Mats for the Reduction of 4-NP. For a catalytic reaction, it is necessary to investigate and discuss its reaction mechanism. Many works have been studied in which the reduction of 4-NP with $NaBH_4$ was catalyzed by a variety of catalysts and have proposed some mechanistic investigations for the reaction process, which can be summed up in the following three major points: (1) adsorption of 4-NP on the surface of the catalysts; (2) enhancement of the ability of electron transfer from BH_4^- to 4-NP; (3) desorption of 4-AP from the surface of the catalysts.[46,48,49] In this work, the excellent catalytic property for the as-prepared $Cu_{2-x}Se/rGO/PVP$ nanofibers according to some of the above studies could be

Table 1. Comparison of the Rate Constants (k) at Different Temperatures for Cu$_{2-x}$Se/PVP, rGO/PVP, and Cu$_{2-x}$Se/rGO/PVP Nanofibers and Corresponding Activation Energies (E_a)

	k (min^{-1})				E_a (kJ/mol, $n = 3$)^a
	25 °C	30 °C	35 °C	40 °C	
Cu$_{2-x}$Se/PVP nanofibers	0.037	0.061	0.10	0.19	86.47 ± 1.22
rGO/PVP nanofibers	0.048	0.070	0.11	0.18	77.32 ± 1.60
Cu$_{2-x}$Se/rGO/PVP nanofibers	0.14	0.17	0.28	0.33	49.05 ± 1.70

^{a}The results of E_a are from Figure 7 (mean ± SD, $n = 3$, n = number of measurements).

attributed to the following three factors (Scheme 1). First of all, the rGO nanofibers have a high adsorptive ability toward the aromatic compound, with 4-NP resulting from π–π-stacking interaction.[41,49] Concomitantly, the strong nucleophile BH$_4^-$ also diffused to the surface of Cu$_{2-x}$Se NPs containing Cu^I and Cu^{II}, which can form a copper hydride complex.[45] In order to demonstrate the adsorption of rGO nanofibers, the BET surface areas of bare PVP, rGO/PVP, and Cu$_{2-x}$Se/rGO/PVP nanofibers based on N$_2$ adsorption experiments were confirmed (Figure S10 and Table S1 in the SI). It is seen that the surface areas of electrospun nanofibers will be larger after the introduction of GO into nanofibers, which could adsorb certain reductants such as 4-NP and NaBH$_4$ into the solution and also provide enough space for the catalytic process. Second, the Cu$_{2-x}$Se NPs with high copper vacancy served as a bridge of the electron acceptor to transfer electrons rapidly from BH$_4^-$ to rGO

nanofibers under daylight as the driving force and then to 4-NP, bringing about the production of 4-AP. BH$_4^-$ with abundant electrons is a strong nucleophile that can facilitate the transfer of electrons from BH$_4^-$ to 4-NP via heterogeneous Cu$_{2-x}$Se NPs/rGO as a synergetic medium in PVP nanofibers. This process as well could help to overcome the kinetic barrier for the reduction of 4-NP.[50] Third, 4-AP desorbed from the Cu$_{2-x}$Se/rGO/PVP nanofibers and diffused into an aqueous solution. Additionally, the whole process was inseparable from the electrospun nanofibers, which provided some active sites and a reactive platform due to its large surface area-to-volume ratio and high porosity. It is adequately demonstrated that the synergetic effect of the Cu$_{2-x}$Se NPs and rGO in PVP nanofibers enhanced its catalytic ability compared with single Cu$_{2-x}$Se/PVP and GO/PVP nanofibers.

Reusability and Stability of Composite Cu$_{2-x}$Se/rGO/PVP Nanofibrous Mats. It is well-known that the sustainable reusability and operating stability are both vital for a good heterogeneous catalyst. So, we have investigated the reusability and stability for composite Cu$_{2-x}$Se/rGO/PVP nanofibrous mats under the same conditions. As depicted in Figure 8, the conversion rate remained 93.5% after five cycles, indicating the eminent recyclability and stability of the composite nanofibrous materials (time-dependent UV–vis spectral changes in Figure S12 in the SI).

Besides, in order to embody the water-stable property of the nanofibrous catalyst, we have also investigated its morphology after different immersion times in a 4-NP/NaBH$_4$ solution. The morphology of the composite nanofibers retained almost unchanged after 7 h in solution, whereas the Cu$_{2-x}$Se NPs in the nanofibers gradually reduced with the immersion time, which can bring about lower activity of the catalysts after the recycle

Scheme 1. Schematic Diagram Illustrating the Synergetic Effect between Cu$_{2-x}$Se NPs and rGO in Electropun Nanofibers for the Reduction Process of 4-NP to 4-AP
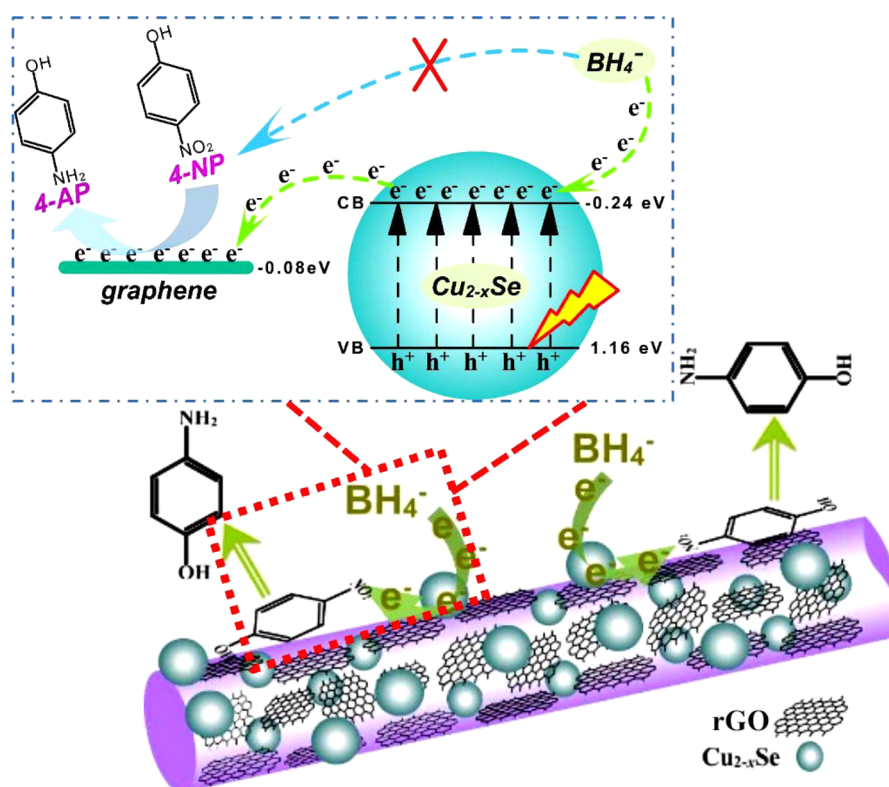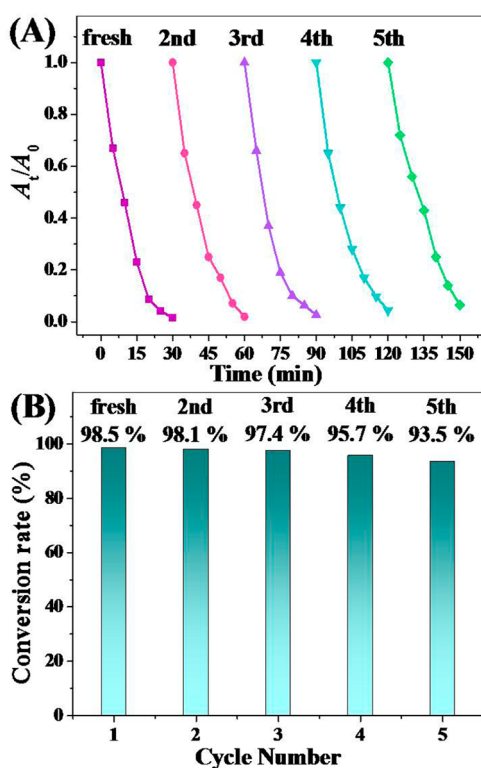
Figure 8. Recycling and reuse of $Cu_{2-x}Se/rGO/PVP$ nanofibrous mats as heterogeneous catalysts for the reduction of 4-NP to 4-AP: (A) A_t/A_0 versus time for the reduction of 4-NP at different reaction times; (B) conversion efficiency of 4-NP in five successive cycles in accordance with part A.

time, consistent with the former reusable tests (Figure S13 in the SI). Consequently, all of the results obviously illustrated that the $Cu_{2-x}Se$ NPs in the nanofibers could be slightly destroyed with reusable cycles. However, the $Cu_{2-x}Se/rGO/PVP$ nanofibrous mats could keep a certain stable property in the whole catalytic process and the conversion rate for the reduction of 4-NP still maintained above 93.5% after five recycles.

CONCLUSIONS

In conclusion, we have successfully exhibited for the first time the preparation of $Cu_{2-x}Se/rGO/PVP$ nanofibers through electrospinning and a simple feasible doping method to mix the semiconductor $Cu_{2-x}Se$ NPs with a GO/PVP electrospun solution. The synthesized composite $Cu_{2-x}Se/rGO/PVP$ nanofibers as catalysts showed the highest rate constant k and the lowest activation energy E_a toward the reduction of 4-NP compared with simplex $Cu_{2-x}Se/PVP$ or rGO/PVP nanofibers. The outstanding catalytic activity of the $Cu_{2-x}Se/rGO/PVP$ nanofibers for the reduction of 4-NP results from the synergetic effect between $Cu_{2-x}Se$ NPs with higher copper vacancy and rGO in the electrospun PVP nanofibers. In this study, the synergetic effect has some intrinsic advantages including improving the charge-transfer rate of the reaction, decreasing the activation energy for the reduction of 4-NP, and providing a number of reaction sites for the reactants. Ultimately, the concept of the synergetic effect in the electrospinning technique will lay a good foundation for the approach of fabricating the composite and multifunctional nanofibers for a broad range of applications in catalysis, biomedicine, chemiluminescence, electrocatalysis, sensors, and so on.

ASSOCIATED CONTENT

S Supporting Information

Additional data and information as noted in the text. The Supporting Information is available free of charge on the ACS Publications website at DOI: 10.1021/acsami.5b03645.

AUTHOR INFORMATION

Corresponding Author

*E-mail: chengzhi@swu.edu.cn. Tel: (+86) 23 68254659. Fax: (+86) 23 68367257.

Notes

The authors declare no competing financial interest.

ACKNOWLEDGMENTS

REFERENCES

(1) Herves, P.; Perez-Lorenzo, M.; Liz-Marzan, L. M.; Dzubiella, J.; Lu, Y.; Ballauff, M. Catalysis by Metallic Nanoparticles in Aqueous Solution: Model Reactions. *Chem. Soc. Rev.* **2012**, *41*, 5577−5587.

(2) Voiry, D.; Yamaguchi, H.; Li, J.; Silva, R.; Alves, D. C. B.; Fujita, T.; Chen, M.; Asefa, T.; Shenoy, V. B.; Eda, G.; Chhowalla, M. Enhanced Catalytic Activity in Strained Chemically Exfoliated WS_2 Nanosheets for Hydrogen Evolution. *Nat. Mater.* **2013**, *12*, 850−855.

(3) Das, S. K.; Parandhaman, T.; Pentela, N.; Maidul Islam, A. K. M.; Mandal, A. B.; Mukherjee, M. Understanding the Biosynthesis and Catalytic Activity of Pd, Pt, and Ag Nanoparticles in Hydrogenation and Suzuki Coupling Reactions at the Nano-Bio Interface. *J. Phys. Chem. C* **2014**, *118*, 24623−24632.

(4) Kumar, M.; Deka, S. Multiply Twinned AgNi Alloy Nanoparticles as Highly Active Catalyst for Multiple Reduction and Degradation Reactions. *ACS Appl. Mater. Interfaces* **2014**, *6*, 16071−16081.

(5) Zhang, P.; Li, R.; Huang, Y.; Chen, Q. A Novel Approach for the in Situ Synthesis of Pt−Pd Nanoalloys Supported on Fe_3O_4@C Core-Shell Nanoparticles with Enhanced Catalytic Activity for Reduction Reactions. *ACS Appl. Mater. Interfaces* **2014**, *6*, 2671−2678.

(6) Mei, Y.; Lu, Y.; Polzer, F.; Ballauff, M.; Drechsler, M. Catalytic Activity of Palladium Nanoparticles Encapsulated in Spherical Polyelectrolyte Brushes and Core-Shell Microgels. *Chem. Mater.* **2007**, *19*, 1062−1069.

(7) Pal, J.; Mondal, C.; Sasmal, A. K.; Ganguly, M.; Negishi, Y.; Pal, T. Account of Nitroarene Reduction with Size- and Facet-Controlled $CuO−MnO_2$ Nanocomposites. *ACS Appl. Mater. Interfaces* **2014**, *6*, 9173−9184.

(8) Zhang, C. L.; Yu, S. H. Nanoparticles Meet Electrospinning: Recent Advances and Future Prospects. *Chem. Soc. Rev.* **2014**, *43*, 4423−4448.

(9) Yang, T.; Yang, H.; Zhen, S. J.; Huang, C. Z. Hydrogen-Bond-Mediated *in Situ* Fabrication of AgNPs/Agar/PAN Electrospun Nanofibers as Reproducible SERS Substrates. *ACS Appl. Mater. Interfaces* **2015**, *7*, 1586−1594.

(10) Yoon, K.; Hsiao, B. S.; Chu, B. Functional Nanofibers for Environmental Applications. *J. Mater. Chem.* **2008**, *18*, 5326−5334.

(11) Rambaud, F.; Vallé, K.; Thibaud, S.; Julián-López, B.; Sanchez, C. One-Pot Synthesis of Functional Helicoidal Hybrid Organic-Inorganic Nanofibers with Periodically Organized Mesoporosity. *Adv. Funct. Mater.* **2009**, *19*, 2896−2905.

(12) Wang, H.; Wang, D.; Peng, Z.; Tang, W.; Li, N.; Liu, F. Assembly of DNA-Functionalized Gold Nanoparticles on Electrospun Nanofibers as a Fluorescent Sensor for Nucleic Acids. *Chem. Commun.* **2013**, *49*, 5568−5570.

(13) Shin, J.; Choi, S.-J.; Lee, I.; Youn, D.-Y.; Park, C. O.; Lee, J.-H.; Tuller, H. L.; Kim, I.-D. Thin-Wall Assembled SnO$_2$ Fibers Functionalized by Catalytic Pt Nanoparticles and their Superior Exhaled-Breath-Sensing Properties for the Diagnosis of Diabetes. *Adv. Funct. Mater.* **2013**, *23*, 2357–2367.

(14) Yang, H.; Huang, C. Z. Polymethacrylic Acid-Facilitated Nanofiber Matrix Loading Ag Nanoparticles for SERS Measurements. *RSC Adv.* **2014**, *4*, 38783–38790.

(15) Li, P.; Wang, C.; Zhang, Y.; Wei, F. Air Filtration in the Free Molecular Flow Regime: A Review of High-Efficiency Particulate Air Filters Based on Carbon Nanotubes. *Small* **2014**, *10*, 4543–4561.

(16) Li, X.; Wang, M.; Wang, C.; Cheng, C.; Wang, X. Facile Immobilization of Ag Nanocluster on Nanofibrous Membrane for Oil/Water Separation. *ACS Appl. Mater. Interfaces* **2014**, *6*, 15272–15282.

(17) Hwang, T. H.; Lee, Y. M.; Kong, B.-S.; Seo, J.-S.; Choi, J. W. Electrospun Core–Shell Fibers for Robust Silicon Nanoparticle-Based Lithium Ion Battery Anodes. *Nano Lett.* **2011**, *12*, 802–807.

(18) Thavasi, V.; Singh, G.; Ramakrishna, S. Electrospun Nanofibers in Energy and Environmental Applications. *Energy Environ. Sci.* **2008**, *1*, 205–221.

(19) Park, M.; Im, J.; Shin, M.; Min, Y.; Park, J.; Cho, H.; Park, S.; Shim, M.-B.; Jeon, S.; Chung, D.-Y.; Bae, J.; Park, J.; Jeong, U.; Kim, K. Highly Stretchable Electric Circuits From a Composite Material of Silver Nanoparticles and Elastomeric Fibres. *Nat. Nanotechnol.* **2012**, *7*, 803–809.

(20) Zhou, F.-L.; Hubbard, P. L.; Eichhorn, S. J.; Parker, G. J. M. Coaxially Electrospun Axon-Mimicking Fibers for Diffusion Magnetic Resonance Imaging. *ACS Appl. Mater. Interfaces* **2012**, *4*, 6311–6316.

(21) Yang, H.; Gao, P. F.; Wu, W. B.; Yang, X. X.; Zeng, Q. L.; Li, C.; Huang, C. Z. Antibacterials Loaded Electrospun Composite Nanofibers: Release Profile and Sustained Antibacterial Efficacy. *Polym. Chem.* **2014**, *5*, 1965–1975.

(22) Kim, Y.-J.; Ebara, M.; Aoyagi, T. A Smart Hyperthermia Nanofiber with Switchable Drug Release for Inducing Cancer Apoptosis. *Adv. Funct. Mater.* **2013**, *23*, 5753–5761.

(23) Senturk-Ozer, S.; Chen, T.; Degirmenbasi, N.; Gevgilili, H.; Podkolzin, S. G.; Kalyon, D. M. A Nanobursa Mesh: A Graded Electrospun Nanofiber Mesh with Metal Nanoparticles on Carbon Nanotubes. *Nanoscale* **2014**, *6*, 8527–8530.

(24) Soukup, K.; Topka, P.; Hejtmánek, V.; Petráš, D.; Valeš, V.; Šolcová, O. Noble Metal Catalysts Supported on Nanofibrous Polymeric Membranes for Environmental Applications. *Catal. Today* **2014**, *236*, 3–11.

(25) Chang, Y.; Han, G.; Li, M.; Gao, F. Graphene-Modified Carbon Fiber Mats Used to Improve the Activity and Stability of Pt Catalyst for Methanol Electrochemical Oxidation. *Carbon* **2011**, *49*, 5158–5165.

(26) Mitschang, F.; Schmalz, H.; Agarwal, S.; Greiner, A. Tea-Bag-Like Polymer Nanoreactors Filled with Gold Nanoparticles. *Angew. Chem., Int. Ed.* **2014**, *53*, 4972–4975.

(27) Lie, S. Q.; Wang, D. M.; Gao, M. X.; Huang, C. Z. Controllable Copper Deficiency in Cu$_{2-x}$Se Nanocrystals with Tunable Localized Surface Plasmon Resonance and Enhanced Chemiluminescence. *Nanoscale* **2014**, *6*, 10289–10296.

(28) Li, W. L.; Lie, S. Q.; Du, Y. Q.; Wan, X. Y.; Wang, T. T.; Wang, J.; Huang, C. Z. Hydrophilic Cu$_{2-x}$Se/Reduced Graphene Oxide Nanocomposites with Tunable Plasmonic Properties and Their Applications in Cellular Dark-Field Microscopic Imaging. *J. Mater. Chem. B* **2014**, *2*, 7027–7033.

(29) Pyun, J. Graphene Oxide as Catalyst: Application of Carbon Materials beyond Nanotechnology. *Angew. Chem., Int. Ed.* **2011**, *50*, 46–48.

(30) Han, C.; Chen, Z.; Zhang, N.; Colmenares, J. C.; Xu, Y.-J. Hierarchically CdS Decorated 1D ZnO Nanorods-2D Graphene Hybrids: Low Temperature Synthesis and Enhanced Photocatalytic Performance. *Adv. Funct. Mater.* **2015**, *25*, 221–229.

(31) Xiang, Q.; Yu, J.; Jaroniec, M. Synergetic Effect of MoS$_2$ and Graphene as Cocatalysts for Enhanced Photocatalytic H$_2$ Production Activity of TiO$_2$ Nanoparticles. *J. Am. Chem. Soc.* **2012**, *134*, 6575–6578.

(32) Ullah, K.; Ye, S.; Lei, Z.; Cho, K.-Y.; Oh, W.-C. Synergistic Effect of PtSe$_2$ and Graphene Sheets Supported by TiO$_2$ as Cocatalysts Synthesized via Microwave Techniques for Improved Photocatalytic Activity. *Catal. Sci. Technol.* **2015**, *5*, 184–198.

(33) Upadhyay, R. K.; Soin, N.; Roy, S. S. Role of Graphene/Metal oxide Composites as Photocatalysts, Adsorbents and Disinfectants in Water Treatment: A Review. *RSC Adv.* **2014**, *4*, 3823–3851.

(34) Shown, I.; Hsu, H.-C.; Chang, Y.-C.; Lin, C.-H.; Roy, P. K.; Ganguly, A.; Wang, C.-H.; Chang, J.-K.; Wu, C.-I.; Chen, L.-C.; Chen, K.-H. Highly Efficient Visible Light Photocatalytic Reduction of CO$_2$ to Hydrocarbon Fuels by Cu-Nanoparticle Decorated Graphene Oxide. *Nano Lett.* **2014**, *14*, 6097–6103.

(35) Liang, M.; Su, R.; Huang, R.; Qi, W.; Yu, Y.; Wang, L.; He, Z. Facile *in Situ* Synthesis of Silver Nanoparticles on Procyanidin-Grafted Eggshell Membrane and Their Catalytic Properties. *ACS Appl. Mater. Interfaces* **2014**, *6*, 4638–4649.

(36) Yang, M.-Q.; Pan, X.; Zhang, N.; Xu, Y.-J. A Facile One-Step Way to Anchor Noble Metal (Au, Ag, Pd) Nanoparticles on a Reduced Graphene Oxide Mat with Catalytic Activity for Selective Reduction of Nitroaromatic Compounds. *CrystEngComm* **2013**, *15*, 6819–6828.

(37) Zhao, Y.; Pan, H.; Lou, Y.; Qiu, X.; Zhu, J.; Burda, C. Plasmonic Cu$_{2-x}$S Nanocrystals: Optical and Structural Properties of Copper-Deficient Copper (I) Sulfides. *J. Am. Chem. Soc.* **2009**, *131*, 4253–4261.

(38) Jabal, J. M. F.; McGarry, L.; Sobczyk, A.; Aston, D. E. Substrate Effects on the Wettability of Electrospun Titania-Poly-(vinylpyrrolidone) Fiber Mats. *Langmuir* **2010**, *26*, 13550–13555.

(39) Choi, J.; Kang, N.; Yang, H. Y.; Kim, H. J.; Son, S. U. Colloidal Synthesis of Cubic-Phase Copper Selenide Nanodiscs and Their Optoelectronic Properties. *Chem. Mater.* **2010**, *22*, 3586–3588.

(40) Riha, S. C.; Johnson, D. C.; Prieto, A. L. Cu$_2$Se Nanoparticles with Tunable Electronic Properties Due to a Controlled Solid-State Phase Transition Driven by Copper Oxidation and Cationic Conduction. *J. Am. Chem. Soc.* **2011**, *133*, 1383–1390.

(41) Hou, J.; Yang, C.; Cheng, H.; Jiao, S.; Takeda, O.; Zhu, H. High-Performance *p*-Cu$_2$O/*n*-TaON Heterojunction Nanorod Photoanodes Passivated with an Ultrathin Carbon Sheath for Photoelectrochemical Water Splitting. *Energy Environ. Sci.* **2014**, *7*, 3758–3768.

(42) Zhang, X.; Zhou, J.; Song, H.; Chen, X.; Fedoseeva, Y. V.; Okotrub, A. V.; Bulusheva, L. G. Butterfly Effect" in CuO/Graphene Composite Nanosheets: A Small Interfacial Adjustment Triggers Big Changes in Electronic Structure and Li-Ion Storage Performance. *ACS Appl. Mater. Interfaces* **2014**, *6*, 17236–17244.

(43) Liu, X.; Lee, C.; Law, W.-C.; Zhu, D.; Liu, M.; Jeon, M.; Kim, J.; Prasad, P. N.; Kim, C.; Swihart, M. T. Au-Cu$_{2-x}$Se Heterodimer Nanoparticles with Broad Localized Surface Plasmon Resonance as Contrast Agents for Deep Tissue Imaging. *Nano Lett.* **2013**, *13*, 4333–4339.

(44) Zhang, Y.; Tang, Z.-R.; Fu, X.; Xu, Y.-J. Engineering the Unique 2D Mat of Graphene to Achieve Graphene-TiO$_2$ Nanocomposite for Photocatalytic Selective Transformation: What Advantage does Graphene Have over Its Forebear Carbon Nanotube? *ACS Nano* **2011**, *5*, 7426–7435.

(45) Huang, C.; Ye, W.; Liu, Q.; Qiu, X. Dispersed Cu$_2$O Octahedrons on *h*-BN Nanosheets for *p*-Nitrophenol Reduction. *ACS Appl. Mater. Interfaces* **2014**, *6*, 14469–14476.

(46) Saha, S.; Pal, A.; Kundu, S.; Basu, S.; Pal, T. Photochemical Green Synthesis of Calcium-Alginate-Stabilized Ag and Au Nanoparticles and Their Catalytic Application to 4-Nitrophenol Reduction. *Langmuir* **2010**, *26*, 2885–2893.

(47) Bhandari, R.; Knecht, M. R. Effects of the Material Structure on the Catalytic Activity of Peptide-Templated Pd Nanomaterials. *ACS Catal.* **2011**, *1*, 89–98.

(48) Feng, J.; Su, L.; Ma, Y.; Ren, C.; Guo, Q.; Chen, X. CuFe$_2$O$_4$ Magnetic Nanoparticles: A Simple and Efficient Catalyst for the Reduction of Nitrophenol. *Chem. Eng. J.* **2013**, *221*, 16–24.

(49) Chen, Z.; Liu, S.; Yang, M.-Q.; Xu, Y.-J. Synthesis of Uniform CdS Nanospheres/Graphene Hybrid Nanocomposites and Their Application as Visible Light Photocatalyst for Selective Reduction of Nitro Organics in Water. *ACS Appl. Mater. Interfaces* **2013**, *5*, 4309–4319.

(50) Bhandari, R.; Knecht, M. R. Effects of the Material Structure on the Catalytic Activity of Peptide-Templated Pd Nanomaterials. *ACS Catal.* **2011**, *1*, 89−98.